An Experimental Investigation of Spin Power Losses of a Turbofan Gearbox

UNDERGRADUATE HONORS THESIS

Presented in Partial Fulfillment of the Requirements for Graduation with Honor's Research Distinction in the Department of Mechanical Engineering at The Ohio State University

By

Kyler McDonald

Undergraduate Program in Mechanical Engineering

The Ohio State University

2017

Thesis Committee:

Dr. Ahmet Kahraman

Dr. David Talbot

Abstract

Planetary gear sets are commonly used in automotive, industrial and aerospace gearbox and transmission applications as they provide certain advantages over their counter-shaft alternatives. Any planetary gear set design must meet multiple requirements of size, weight, noise, load carrying capacity, fatigue life, noise, and efficiency. Planetary gear set efficiency is dictated by two classes of power losses. One class includes load dependent power losses that are induced by friction of contact interfaces and they can be predicted using physics-based models. The other class includes load independent losses that are due to interactions of the fluid with rotating gear components. These spin losses are transmission specific and become significant at elevated speeds as in aerospace applications. This experimental study aims at measurement of spin losses of a jet engine turbofan gearbox under realistic speed and temperature and lubricant flowrate conditions. A dynamometer set-up that can operate a turbofan gearbox at speeds up to 10,000 rpm will be developed. The set-up will be incorporated with a forced lubrication system for delivery of lubricant to desired locations at specified flowrates. Torque provided to the gearbox will be measured as a function of rotational speed to determine the spin losses of the gearbox. Additional tests will be performed with subsets of the gearbox to quantify the contributions of spin power loss components such as drag and gear mesh pocketing.

Dedication

To my family and friends who supported me and helped me achieve my goals.

Acknowledgements

I would like to thank my advisor Dr. Kahraman for allowing me to take on this research project along with his support and guidance during this project. I also would like to thank Isaac Hong for his continuous support and extensive help during this project. Thank you to all of my colleagues for their help and generosity to help me with any task I needed. I also want to extend my thanks to Sam Shon for offering me a position in the GearLab as an undergraduate which allowed me to take on this amazing opportunity.

Finally, I want to thank my friends for their infinite support, and to my family for always pushing me to achieve my goals and dreams, without them none of this would've been possible.

Vita

1994.....Born in Vandalia, Ohio

May 2012.....Vandalia-Butler High School

Vandalia, Ohio

May 2015 to Present…….....Research Associate, GearLab

Fields of Study

Major Field: Mechanical Engineering

Table of Contents

List of Tables

List of Figures

Chapter 1:

Introduction

1.1 Background and Motivation

Planetary gear sets are widely used in automotive, industrial and aerospace gearbox and transmission applications. They are preferred over their counter-shaft alternatives since they are more compact and quiet. In addition, their coaxial designs minimize the need for support bearings in the process introducing a self-centering capability to reduce sensitivity to manufacturing errors. As for single gear pairs, design of planetary gear sets is dictated by a set of requirements for weight and size, load carrying capacity, fatigue life, noise and efficiency. While the other requirements can be met by using the knowledge and tools developed for a gear pair, efficiency of planetary gear sets is more involved because there are various contributors. It not only defines energy waste during power transmission also determines heat generated in the gear box that must be removed through proper lubrication systems.

In their theoretical [1] and experimental [2] studies, Talbot and Kahraman defined total power losses as a sum of two categories of losses. One category consists of friction

induced losses taking place along the gear and bearing contact surfaces under load. These losses are referred to as load-dependent or mechanical losses, P_m. The other group of losses is not related to load and originate from interactions of rotating gearbox components with the fluid medium around them. These losses are known as load-independent or spin power losses, P_s. The total power loss *P* of the planetary gear set is then given by

$$P = P_m + P_s \tag{1}$$

As the applications studied in Refs. [1], [3] were automotive power transmission (0-4000 rpm sun gear speed), operating speeds were moderate such that P_m constitutes a large portion of *P*. In cases when speeds increase further (up to 6000 rpm sun gear speed), P_s becomes a larger contributor, as studied experimentally by Kahraman et al [4]. This study showed that there are multiple components to P_s, namely drag losses of gears of the planetary gear set (sun, ring and a set of planets), P_{dg}, drag loss of the planet carrier, P_{dc} pocketing losses [5] of sun-planet and planet-ring gear meshes, P_p, and other spin losses associated with the planet bearings, P_b, and seals, P_s:

$$P_s = P_{dg} + P_{dc} + P_p + P_b + P_s \tag{2}$$

Kahraman et al. [4] concluded that P_p component is lower compared to the drag and bearing loss components, in part, because the operating speeds were still moderate in comparison to those used in aerospace applications. Predictions from Talbot et al. [5] of pocketing losses suggest that they would be the dominant loss component at aerospace

speed conditions. There is no high-speed planetary gear power loss set data available in the literature. As models like Ref. [5] are largely invalidated, the main focus of this study is to develop a high-speed (6000-12000 rpm sun gear speed) test setup and conduct spin power loss experiments on planetary gear sets.

1.2 Literature Review

1.2.1 Spin Power Loss Components

The components of spin power loss consist of bearing, drag, and pocketing power losses as mentioned in section 1.1. Past research has been performed to determine these individual components and their effects on different gearing systems. Harris [6] was able to determine a empirical formulae that has been used by many to determine the bearing loss component of spin power loss. Studies into drag power loss have mostly consisted of windage studies. Studies by Wild et al. and Akin et al. [7], [8] investigated single gears spinning in air and jet lubrication respectively. Another study by Dawson investigated windage losses in larger gears at high speeds, and it was determined from this study that windage power loss was significant at higher speeds [9]. A similar study by Diab et al. looked at windage losses in high speed gears as well, and his conclusions matched that of Dawson's [10]. Along with all of these experimental investigations, Seetharaman and Kahraman were able to develop of a windage power loss model for spur gears. Their first model looked at drag on the periphery and face of spur gears [11] and a similar study developed a model for windage based on gear geometry, operating conditions and lubricant properties. Pocketing power loss investigations by Diab et al. looked at pumping loss

effects on high speed spur and helical gears [10], [12]. These studies showed that pumping (pocketing) losses were indeed a significant contributor to the power loss at high speed applications.

1.2.2 Spin Power Losses of a Planetary Gear Set

As mentioned in section 1.2.2 there have been many studies into the effects of spin power loss. However, these studies have looked at fixed gear systems, and not at the effects of spin power loss in planetary gear systems.

Currently there have been a few studies performed to evaluate the spin power loss contributions in planetary gear sets. One of the main studies in spin power loss components of planetary gear sets was by Hilty. His investigation showed that the overall spin power loss of planetary sets was a combination of the individual spin loss components [13]. Kahraman et al. [4] showed that viscous bearing and pocketing losses were the primary spin loss components followed by drag power loss.

Another main study by Talbot et al. explored the efficiency of planetary gear sets. This study investigated both load dependent and load independent power loss components of planetary gear sets. Talbot's study was able to determine that increasing planet gears into the system increased the overall spin power loss [3]. Talbot et al. also created a pocket power loss model for helical gears in planetary configurations [5]. It was also found that as lubrication temperatures used increase the overall spin power loss decreases [3], [4].

All of these studies are very significant in understanding the spin power loss contributions of planetary gear sets. However, all of these studies have focused on the automotive application of planetary gear sets where sun gear speeds are below 4000 RPM. This study will investigate the individual components of spin power loss in an aerospace application with speeds up to 10000 RPM.

1.3 Objectives and Scope

The main objectives of this thesis are listed as follows:

- Develop and run off a high speed test set up and related efficiency instrumentation and data acquisition systems.
- Execute a test matrix covering ranges of operating speeds and quantify their impact on spin power losses.
- Perform experiments with various subsets of the test setup in an attempt to break down the spin losses to its components as defined in Eq. (2)

The scope of this thesis will be limited to spin power loses of planetary gear set consisting of a double helical sun gear and two planet gears. The methodology and results of this study will be used to form a baseline for an MS thesis exploring the power losses from gear pocketing.

1.4 Outline

Chapter 2 introduces the experimental test setup and procedures. It provides a testing matrix that will be executed along with data acquisition systems and testing conditions. A further explanation of the testing conditions and data analysis systems used in this study will be provided.

Chapter 3 introduces the results from experimentation, followed by individual power loss components and analysis of their effect on the efficiency of the system. This chapter will elaborate on the torque measured for each test and use these torque measurements to calculate the power loss of the planetary gear set.

Chapter 4 will summarize the results of this study and draw on a number of conclusions found from this study along with a prelude to the Master's thesis to follow.

Chapter 2

Experimental Methodology

2.1 Introduction

This chapter introduces the experimental methodology developed in this study to quantify load-independent power losses of a sub-set of a jet engine turbofan gearbox. It describes the test dynamometer, the dedicated test set-up developed particularly for this study, test gear box, and measurement systems devised. It also describes data analysis details as well as the influence of various factors such as bearing housing temperatures on the spin losses of the gear set. A test matrix is defined that is designed towards quantifying the various power loss components such as bearings, gear drag and gear mesh pocketing. Results of limited repeatability studies are also presented to assess the accuracy of the measurements to be presented in the next chapter.

2.2 Test Setup

A general-purpose transmission test dynamometer is used as the test bed in this study. Figure 2.1 shows an overall view of this dynamometer, excluding its auxiliary units

such as the control unit and the external forced lubrication system. It consists of a 250 HP AC drive motor mounted on an isolated test bed. The test bed is covered by a safety cabin. This drive is able to provide the power to the test bed at speeds up to 4000 rpm. As this study is concerned only with the load-independent (spin) power losses, there is no need to use a brake in this setup such that the power capacity of this drive is more than required.

Jet engine turbofan gearboxes consist of a planetary gear set in a fixed (stationary carrier) or star configuration. In this arrangement, the sun gear is the highest speed component and the ring gear is the lowest speed component. Acting as idler gears between the sun and ring are a set of identical planet gears (also called star gears), typically five of them, forming parallel power flow branches. A typical jet engine turbofan gear set in this configuration is shown in Figure 2.2. Testing of an entire turbofan gear set (sun, *N* planet on a stationary carrier and the ring gear) on the dynamometer of Figure 2.1 is not feasible for various reasons including the following:

- Testing of a complete gearbox would require special hoists and fixtures to mount the gearbox on the dynamometer bed as its weight makes it impossible to lift it manually.

- The actual turbofan gearbox uses journal bearings for the planet gears while floating the sun gear radially. Journal bearings require large flow rates of lubricant to be supplied at high temperatures and supply pressures that is beyond the capacity of the auxiliary lubrication system that accompanies the dynamometer.

- Use of journal bearings in the gearbox would also require that the gearbox must transmit sizable amounts of power. These kinds of bearings are not designed to be run under no load conditions. They must be loaded to operate properly. If one were to run tests under loaded conditions, the load-dependent power losses would also be present. Such losses would then be isolated and removed since this study is concerned with only load-independent spin losses. In reality, the drive unit of the dynamometer of Figure 2.1 would not be sufficient to deliver required levels of power and a very large capacity brake would be required.

For these practical reasons, a sub-set of an actual turbofan gearbox will be considered in this study with the following revisions:

- Journal bearings of planet (star) gears will be replaced by rolling element bearings such the set-up can be run without a large capacity lubrication system as well as without a brake.

- The sun gear will also be supported by rolling element bearings such that the complications associated with radial floating of the sun gear is avoided.

Per previous experimental and theoretical investigations on planetary gear sets [1-2], [4], various components of spin power losses of a planetary gear set can be treated as independent sources, with the sum of these component losses forming the total spin loss. With that the total spin power loss of the turbofan gear set shown in Figure 2.2 can be written as ($N = 5$ in Figure 2.2 since there are five planets)

$$P = P_{s,d} + P_{r,d} + NP_{p,d} + NP_b + NP_{sp,poc} + NP_{rp,poc}\,. \tag{2.1}$$

Here $P_{s,d}$ $P_{r,d}$ and $P_{p,d}$ are the drag power losses of the sun, ring and planet gears, respectively. They occur because of the churning of the medium (a mixture of oil and air) by these rotating gears [5], [11]. P_b is the spin loss associated with a journal bearing supporting a planet gear. Finally, $P_{sp,poc}$ and $P_{rp,poc}$ are the power losses associated with pumping of the medium from the sun-planet and ring-planet gear mesh interfaces, respectively [5], [11-12].

As the main focus here is on the drag losses of the high-speed components, namely the sun planet gears as well as the pocketing losses occurring at the gear meshes, (i.e. components $P_{s,d}$, $P_{p,d}$ and $P_{sp,poc}$ in Equation (2.1)), a sub-set of a system like the one shown in Figure 2.2 is suitable here. For this reason, a three-gear arrangement from another study of the sponsor is adapted here. Figure 2.3(a) shows this sub-set consisting of a sun gear and two of the planet gears positioned at an angle of 72 degrees from each other around the sun gear since they came from a 5-planet gear set. In this arrangement, Equation (2.1) reduces to

$$P = \underbrace{P_{s,d} + 2P_{p,d}}_{\substack{sun\ and \\ planet\ drag}} + \underbrace{P_{s,b} + 2P_{p,b}}_{bearings} + 2P_{sp,poc}\,. \tag{2.2}$$

Figure 2.4 shows the fixtures to operate this three-gear sub-set in required operating conditions. Figure 2.5 shows a solid model of the same while Figure 2.6 presents a top-view schematic of it with the main components of the set-up labeled. The following main components are noted:

- A rigid spindle support is connected to the drive motor shaft on the input side which also support one of the pulleys of a 3:1 ratio belt drive in order to increase the maximum speed comfortably to 10,000 rpm, a speed range typical of geared turbofan sun gears.

- Another spindle support is on the high-speed side support other pulley rigidly. The same support table also holds a torque-meter, shown in Figure 2.8(a) that is connected to the high-speed spindle via a flexible coupling such that the torque sensor is isolated from any radial forces and twisting moments.

- The output shaft of the torque sensor is connected to a massive shaft that is designed to hold the sun gear at the end. This connection is again established using a flexible coupling to protect the torque sensor.

- An input shaft whose assembly cross-section is shown in Figure 2.7(a), is supported by two bearing cartridges. The cartridge next to the sun gear houses a pair of angular contact ball bearings while the cartridge on the torque sensor side contains a cylindrical roller bearing. Both bearing cartridges were sealed such that they can be operated under dip lubricated conditions. Also note that the sun gear shaft is hollow with passages designed to route cables to a slip ring as future work includes measurement of pocketing pressure at the sun gear meshes via pressure sensors.

- Likewise, as shown in Figure 2.7(b), each planet gear is supported by a massive shaft held by two bearing cartridges containing cylindrical roller bearings identical to that of the back cartridge of the sun shaft.

- Two vertical support flanges hold all six bearing cartridges as shown in Figure 2.4. Additional plates connect these flanges horizontally to increase the rigidity of the support.

The test gears used in this study, as shown in Figure 2.3(a), were borrowed from a prototype turbofan gearbox. They are double helical gears. The sun gear has 34 teeth at a pitch diameter of 171.4 mm. The planet gears have 31 teeth at a pitch diameter of 156.3 mm.

2.3 Measurement Systems

The main parameter that needed to be controlled in this set-up was the input speed. The speed controller of the dynamometer drive was precise enough to maintain a constant input speed well within 1% of the set value with negligible fluctuations.

Two sets of measured parameters were the torque provided to the gearbox that is the torque signal output by the torque-meter as shown in Figure 2.8(a). This torque sensor (Himmelstein MCRT 49703V(5-2)) has a maximum torque range of 56 Nm (500 lbf-in), a maximum speed of 10,000 rpm, and a resolution of 0.05% of the maximum torque range (about 0.03 Nm). The raw torque and RPM data was sent to a computer where it was analyzed and recorded by a custom program.

A typical raw torque signal measured by the sensor is shown in Figure 2.9 with speed increment labeled on it for clarity. It consists of 9 speed increments starting at $\Omega = 9,000$ rpm, slowing down to 1000 rpm at the increments of 1000 rpm. The set-up is

run for one-minute long segments at each constant speed increment and the arithmetic average of the torque signal over this period was computed to represent the torque loss T at that speed. With that the power loss at that speed was determined as

$$P = \frac{2\pi}{60} T\Omega \tag{2.3}$$

where Ω is in rpm and T is in Nm resulting in P in Watts. A constant reference power loss value of P_{ref} was used to normalize all power loss measurement such that

$$\bar{P} = \frac{P}{P_{ref}}. \tag{2.4}$$

During the preliminary measurements, the repeatability of the measured torque value at a given speed was seen to be poor. The main reason for this was found to be the sensitivity of the bearing spin losses (term $P_{s,b} + 2P_{p,b}$ in Equation (2.2)) to operating temperatures of the bearings. As bearing pedestals were sealed with their own dip lubrication, their temperatures are not controlled. As such depending on the temperatures of these bearings, the measured torque level was altered. This obviously cannot be tolerated here as the main concern, drag and pocketing losses, could not be removed from the bearing losses. As such, each bearing pedestal was equipped with a thermocouple as shown in Figure 2.8(b). J-Type thermocouples were used for this purpose. As illustrated in Figure 2.10, thermocouple signals were connected to a NI 9211 C series temperature input module. The temperature module was connected to a NI cDAQ-9174 chassis which was then connected to the computer to determine temperatures. Figure 2.11 shows example temperature time histories from front and back bearing cartridges of the sun gear shaft. For this particular

case, the front and back bearings of the sun shaft are seen to reach steady-state temperature values of $100^{\circ}C$ and $65^{\circ}C$ after nearly 500 seconds of testing in this particular condition.

Figure 2.12 shows various torque measurements at different front bearing temperature values. The measured torque value at $76^{\circ}C$ is 5.35 Nm while it is reduced to 4.83 Nm (10% lower) at $103^{\circ}C$. To avoid such variations, all the tests performed in this study made sure that the front bearing temperature is within the $95-105^{\circ}C$ range within which the measured torque values are repeatable.

2.4 Lubrication System

In order to be able to add facilities to visualize the oil flow and perform flow collection studies, the sponsor of this project designed a plastic gearbox housing that is bolted to one of the vertical flanges as shown in Figure 2.3(b). This housing has various geometric features to replicate the oil flow conditions within the actual turbofan gearbox. It allows the oil to be provided at various locations including at two spray bars and a number of side entry ports to simulate the journal bearing oil discharge effects. One spray bar and one of the side ports were chosen as the lubricant delivery points in this study.

The lubrication system is shown in Figure 2.13. A 2 HP (AMT-T63CSDPT) pump was used to apply lubrication to the system. The flow was measured in L/min using a GPI-LM50D flow-meter. A custom designed lubrication collection pan was fabricated and used to funnel the lubricant into a scavenger pump which returned to oil the pump reservoir. This lubrication system was not equipped with any heaters or heat exchangers to regulate

the temperature of the lubricant. Further no attempt was made to increase the oil inlet temperature to representative oil inlet temperatures in a turbofan that ranges from $130^{\circ}C$ to $160^{\circ}C$. Operating with a heated oil at these temperatures was not possible since the housing material was plastic. Yet, measurements with oil supplied at room temperature should be expected to be very different than those at the actual intended temperatures due to the effect oil viscosity has on spin losses. In order to overcome this problem, a synthetic (Sim 3.6 CST) was used as lubricant here. This compound can be formulated to have a viscosity at room temperature that is equal to the viscosity of the engine oil at a desired actual temperature. With the formulation used here, viscosity and density of the engine oil at $150^{\circ}C$ was simulated at room temperature.

Also shown in Figure 2.3 are oil inlet locations. Here a total flow rate of 6.7 L/min was used in all tests with 2.7 L/min of it applied to spray bar 1 while the remaining 4.0 L/min applied to the side port.

When testing at higher speeds, there was significant misting coming from the heated lubrication in the gearbox. A mist collection system was devised to collect this mist to maintain the air quality and visibility within the test chamber.

2.5 Test Matrix

According to the test matrix of Table 2.1, the first test includes the sun gear shaft with no sun gear and the transmission cover as shown schematically in Figure 2.14(a). With the assumption that the windage losses associated with the sun gear shaft are

negligible, the power loss measured through configuration I can be assumed to be the sum of the spin losses of the front (subscript *sf*) and back or rear (subscript *sr*) bearings of the sun shaft as shown in the cross-section view of Figure 2.7(a). Mathematically

$$P_I = P_{sf,b} + P_{sr,b} = P_b \tag{2.5}$$

where P_I is the measured power loss for configuration I, and $P_{sf,b}$, $P_{sr,b}$ are the losses of the front and back bearings of the sun gear shaft, respectively.

As depicted in Figure 2.14(b), configuration II in Table 2.1 adds the sun gear to the sun shaft as well as placing the gearbox cover and applying the lubricant to the system such that the measured power loss P_{II} includes not only the bearing losses of the sun shaft as in configuration I but also drag losses associated with windage of the sun gear such that

$$P_{II} = P_{s,d} + \underbrace{P_{sf,b} + P_{sr,b}}_{sun\ bearings}. \tag{2.6}$$

Here $P_{s,d}$ is the drag power loss of the sun gear that can be estimated as the difference of losses from configurations II and I as

$$P_{s,d} = P_{II} - P_I \tag{2.7}$$

according to Eq. (2.5) and (2.6).

The next set of tests in the test matrix of Table 2.1 use configuration III (Figure 2.14(c)) where a planet gear is added to the setup from configuration II along with the lubrication. The measured power loss P_{III} includes not only bearing and drag losses of the

sun gear as in configuration II but also bearing and drag losses of the planet gear along with pocketing loss from the gear mesh such that

$$P_{III} = P_{s,d} + \underbrace{P_{sf,b} + P_{sr,b}}_{sun\ bearings} + P_{p,d} + \underbrace{P_{pf,b} + P_{pr,b}}_{planet\ bearings} + P_{sp,poc} \tag{2.8}$$

With the assumption that losses on sun shaft bearing are nearly equal to the planet shaft bearings

$$\underbrace{P_{sf,b} + P_{sr,b}}_{sun\ bearings} \approx \underbrace{P_{pf,b} + P_{pr,b}}_{planet\ bearings} = P_b\,, \tag{2.9}$$

one can write

$$P_{III} = 2P_b + P_{s,d} + P_{p,d} + P_{sp,poc} \tag{2.10}$$

where $P_{sp,poc}$ is the pocketing power loss of the gear mesh between the sun and planet gear. Further assuming that drag losses on the sun gear are equal to the drag losses of the planet gear since their sizes and rotational speeds are within 10% of each other

$$P_{s,d} \approx P_{p,d} \equiv P_d \tag{2.11}$$

then

$$P_{III} \approx 2P_b + 2P_d + P_{sp,poc}\,. \tag{2.12}$$

With this, pocketing loss is estimated as

$$P_{sp,poc} = P_{III} - 2P_{II}\,. \tag{2.13}$$

The final set of tests in the test matrix of Table 2.1 use configuration IV where a second planet gear is added to setup used for configuration III along with the lubrication as shown in Figure 2.14(d). The measure power loss P_{IV} includes bearing and drag losses for the sun and both planet gears along with pocketing losses from the two gear meshes such that

$$P_{IV} = \underbrace{P_{sf,b} + P_{sr,b}}_{\text{sun bearings}} + P_{s,d} + \underbrace{2\left(P_{pf,b} + P_{pr,b}\right)}_{\text{planet bearings}} + 2P_{p,d} + 2P_{sp,poc} \tag{2.14}$$

Using the same assumptions for bearing and drag losses that were used for configuration III

$$P_{IV} \approx 3P_b + 3P_d + 2P_{sp,poc}. \tag{2.15}$$

With the aid of above test content from the first three configurations, individual power loss components $3P_b$, $3P_d$, and $2P_{sp,poc}$ of P_{IV} can be estimated and inserted in Eq. (2.15) to estimate P_{IV}. At the same time, the direct measurements from configuration IV provide the actual value of P_{IV} that can be compared to the estimated value to assess the accuracy of the above scheme of partitioning the power loss to its components.

Table 2.1: Test matrix conducted in this study.

Configuration	Hardware content	Oil Supply Location	Oil Type
I	Sun shaft only	-	air
II	Sun, sun	-	air
III	Sun, Planet-1	Spray bar 1	Sim 3.6 CST
IV	Sun, Planet-1, Planet-2	Spray bar 1	Sim 3.6 CST

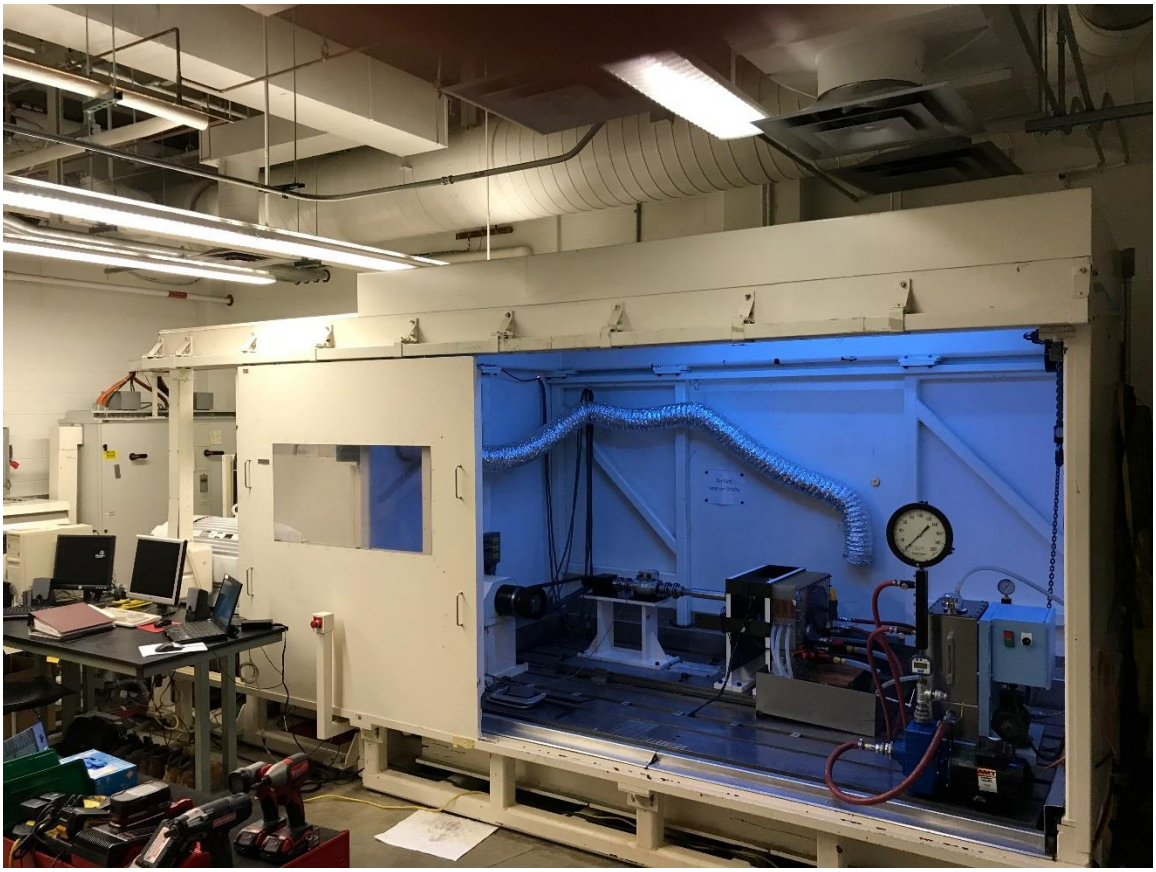

Figure 2.1: Transmission dynamometer used in this study.

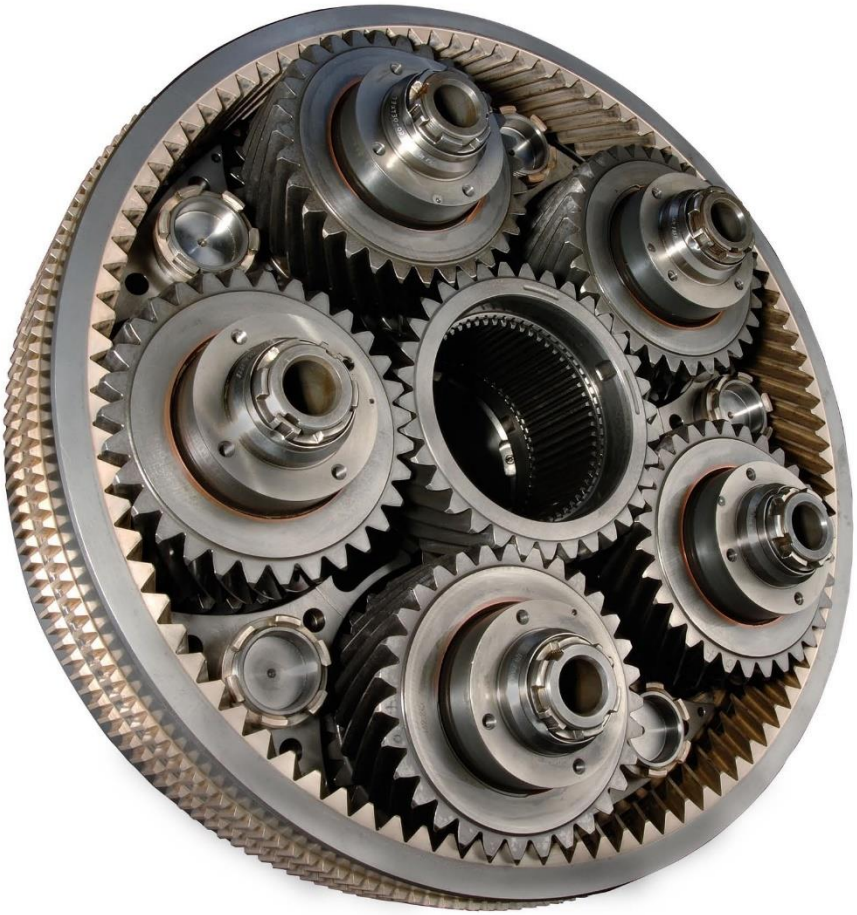

Figure 2.2: An example turbofan planetary gearbox with five double-helical planet (star) gears. [14]

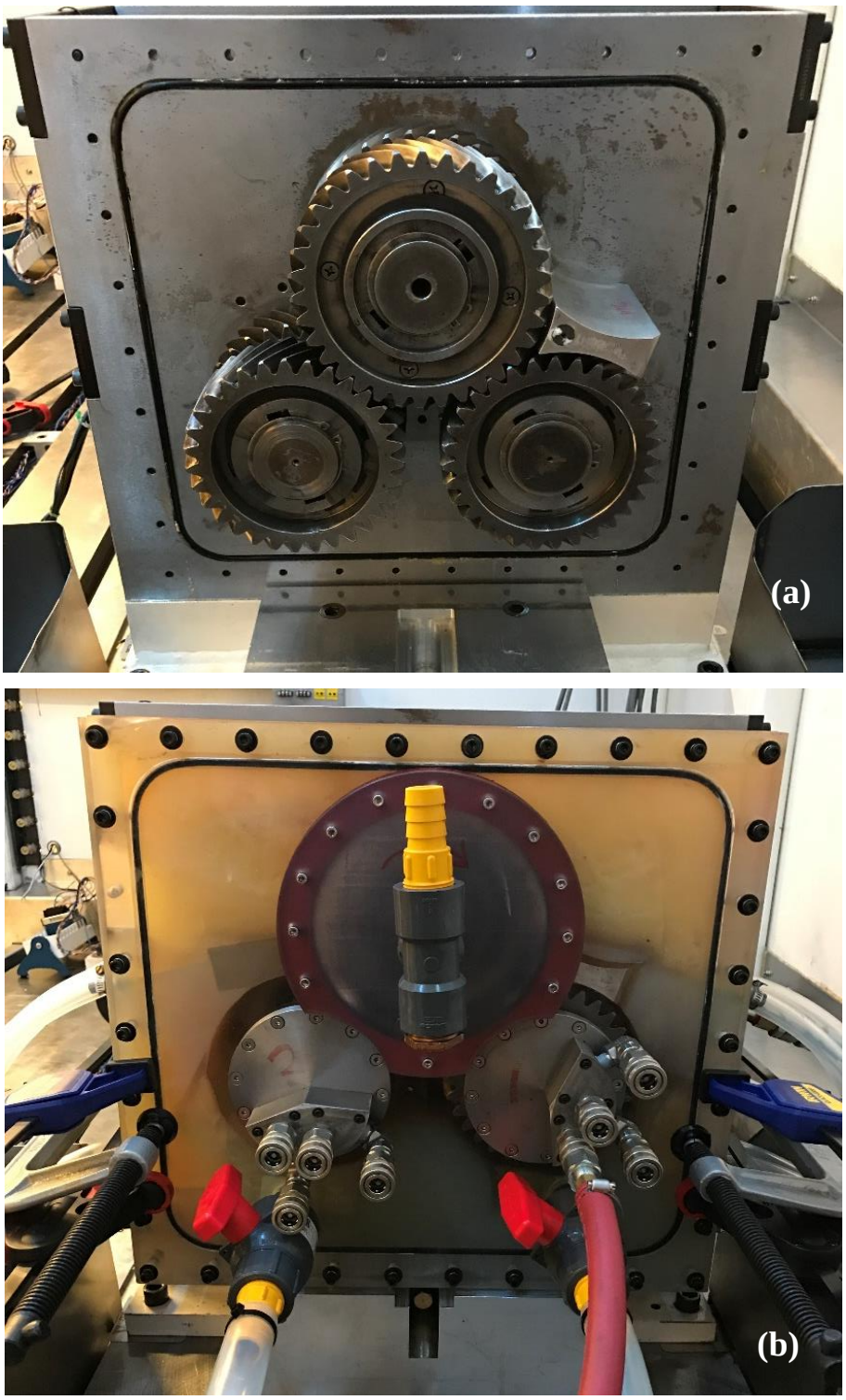

Figure 2.3:(a) Sub-set of a turbofan gearbox with the sun gear and two planets used in this study; (b) the same set-up with the plastic housing mounted

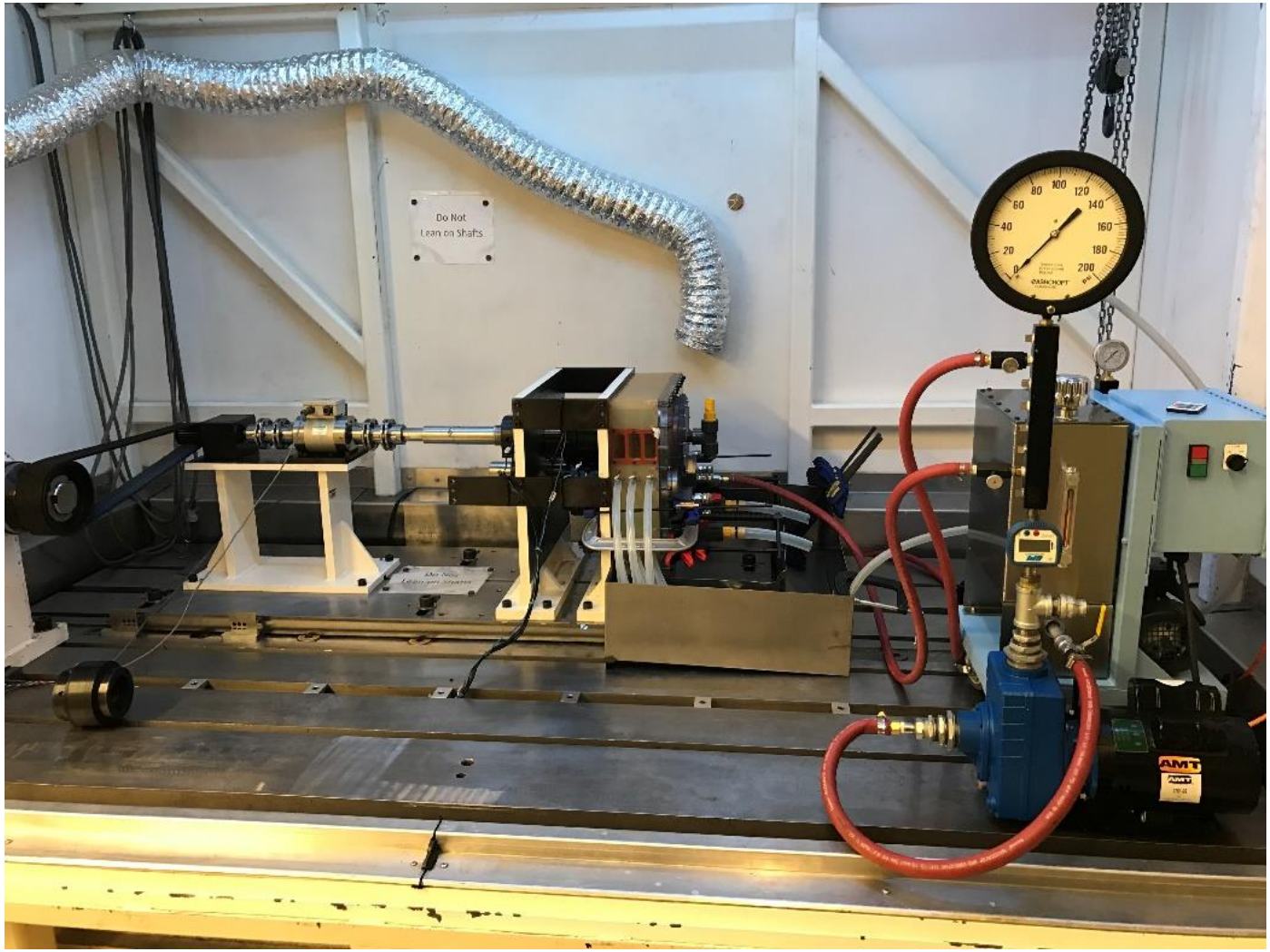

Figure 2.4: Test set-up and its lubrication system on the test bed of the dynamometer of Figure 2.1

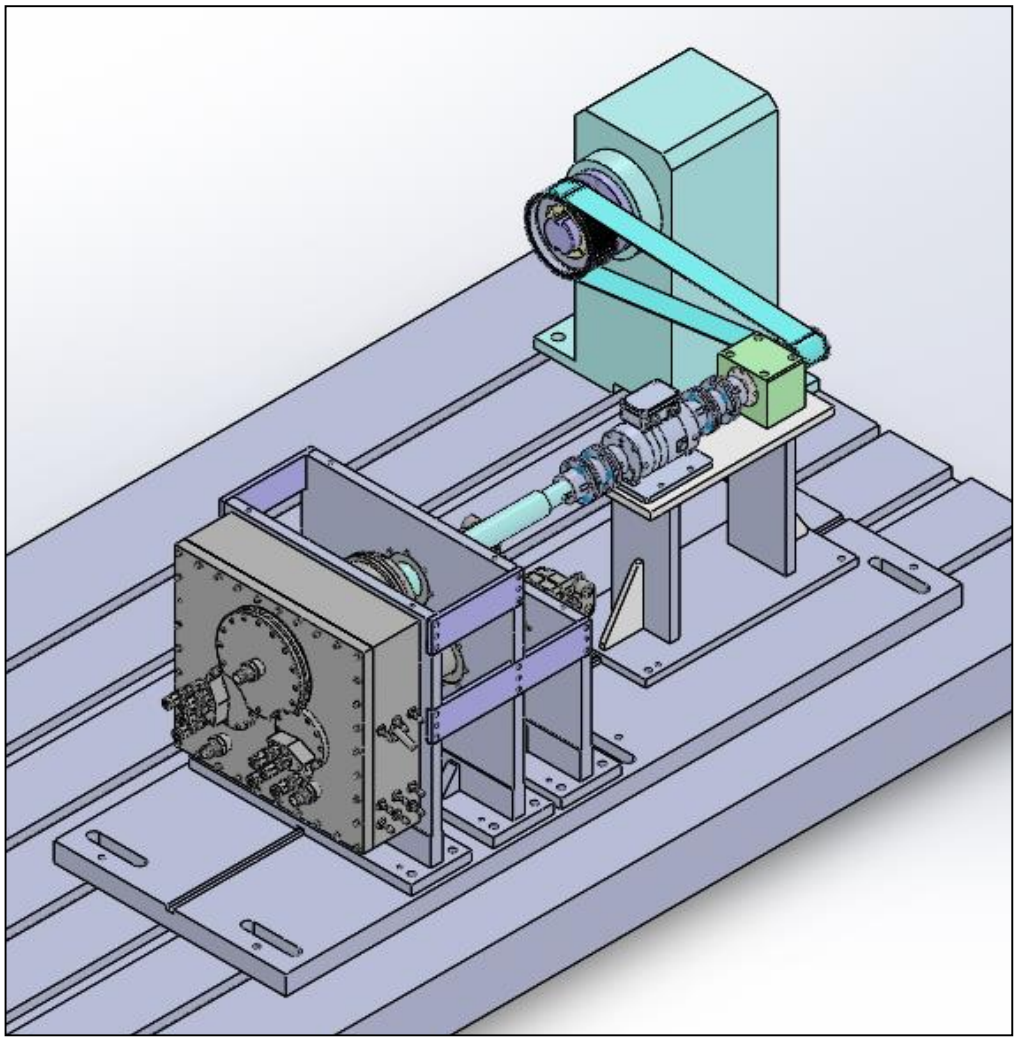

Figure 2.5: Solid model of the test fixtures developed for this study

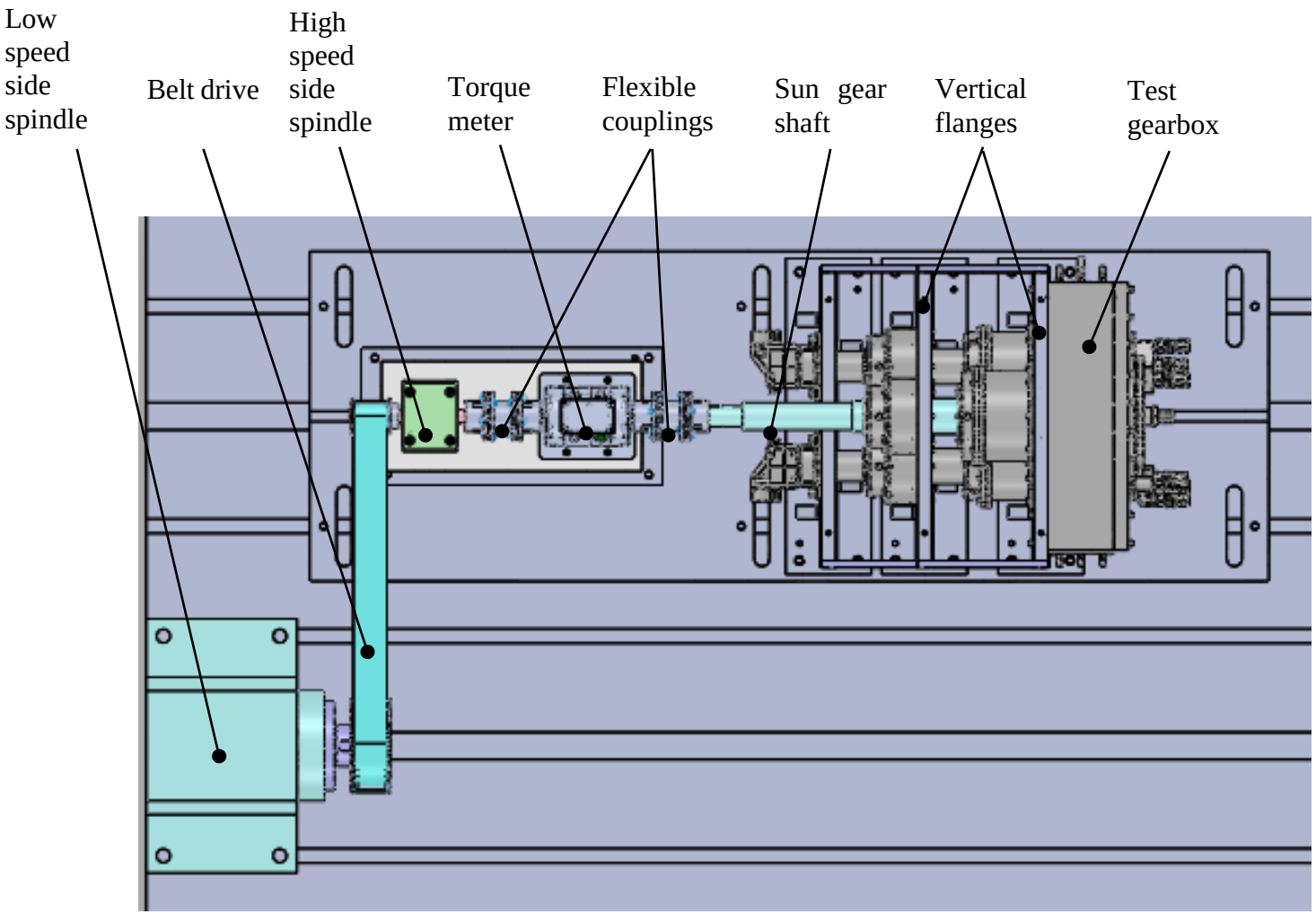

Figure 2.6: Top view of test fixtures with key components labeled.

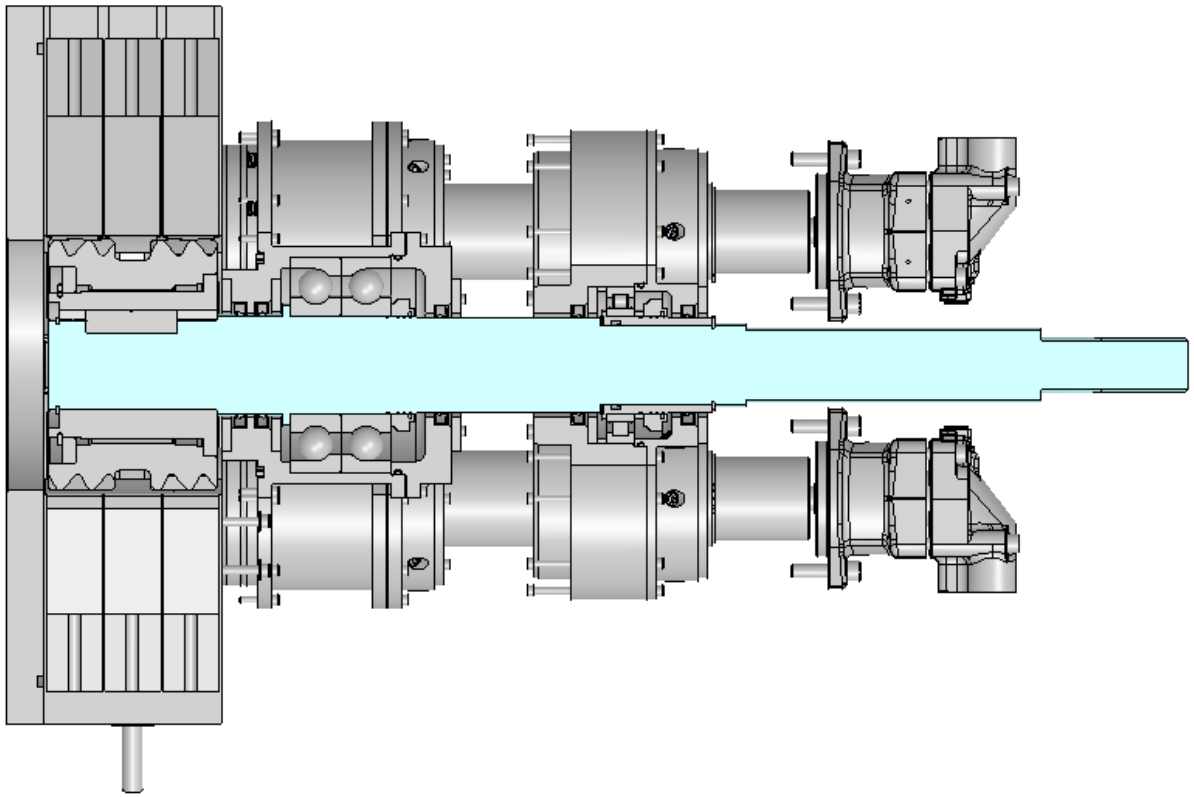

(a)

Figure 2.7: Top cross-sectional view showing (a) the sun gear shaft assembly and (b) planet gear shaft assemblies.

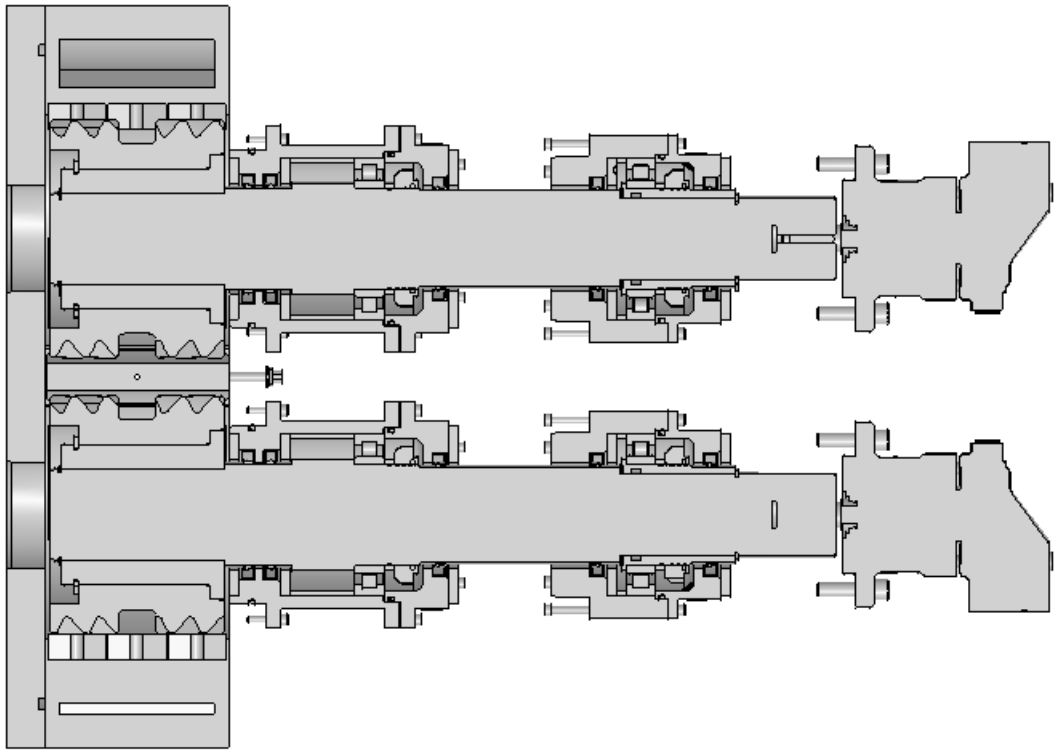

(b)

Figure 2.7: Continued.

(a)

(b)

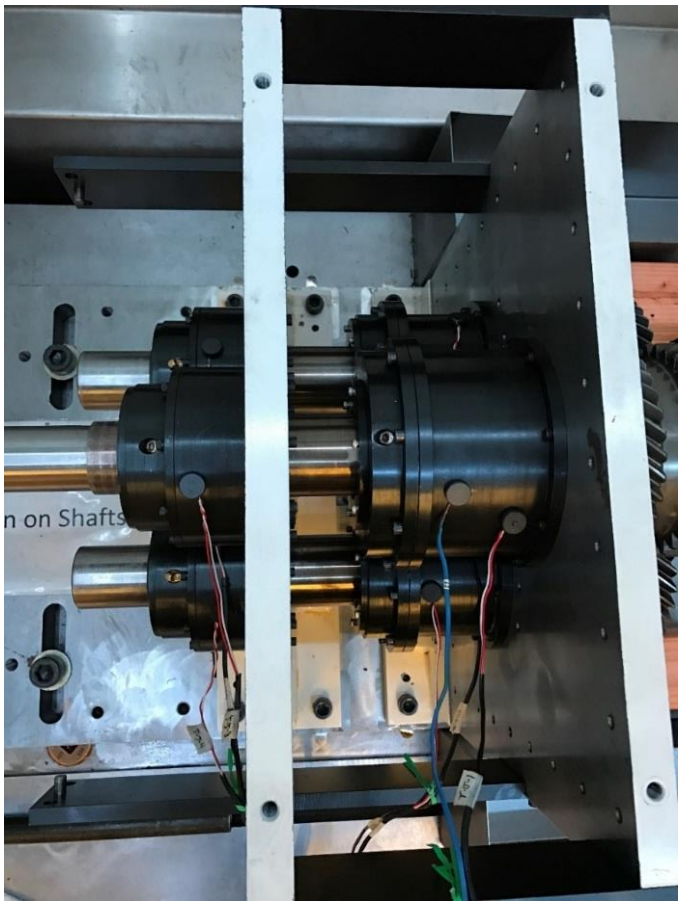

Figure 2.8: Views of (a) the torque sensor and (b) thermocouples mounted on bearings cartridges.

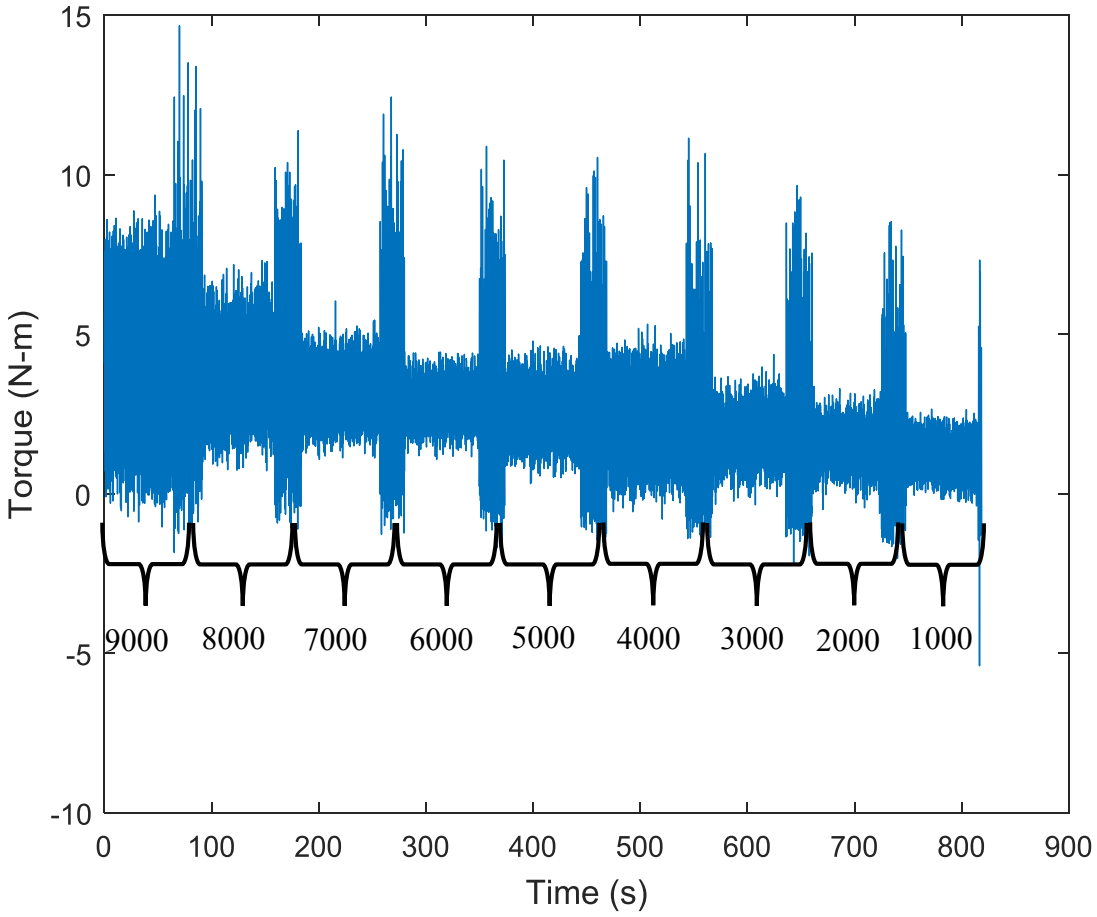

Figure 2.9: An example of raw torque signal as a function of time at different rotational speeds.

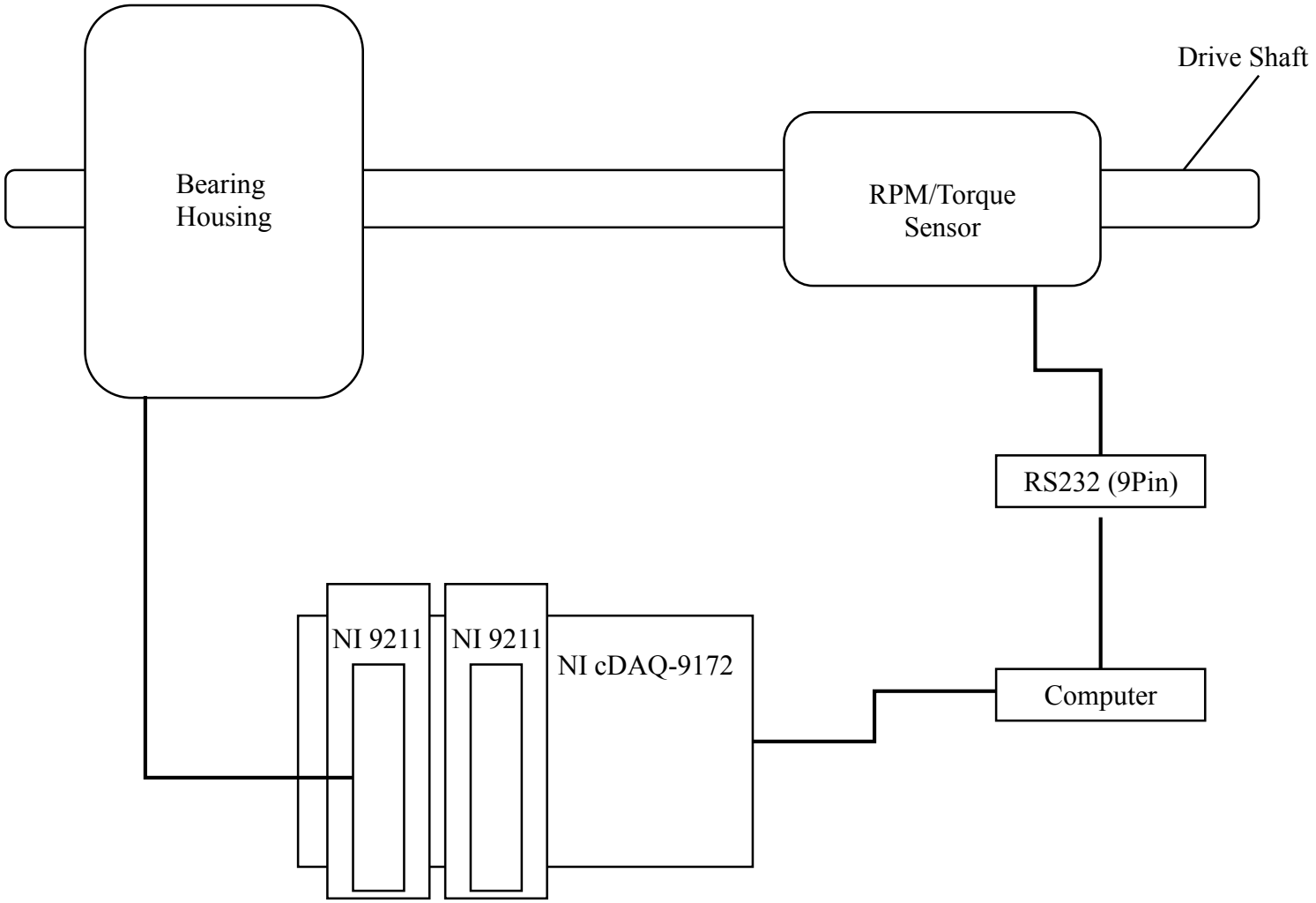

Figure 2.10: Measurement system schematic

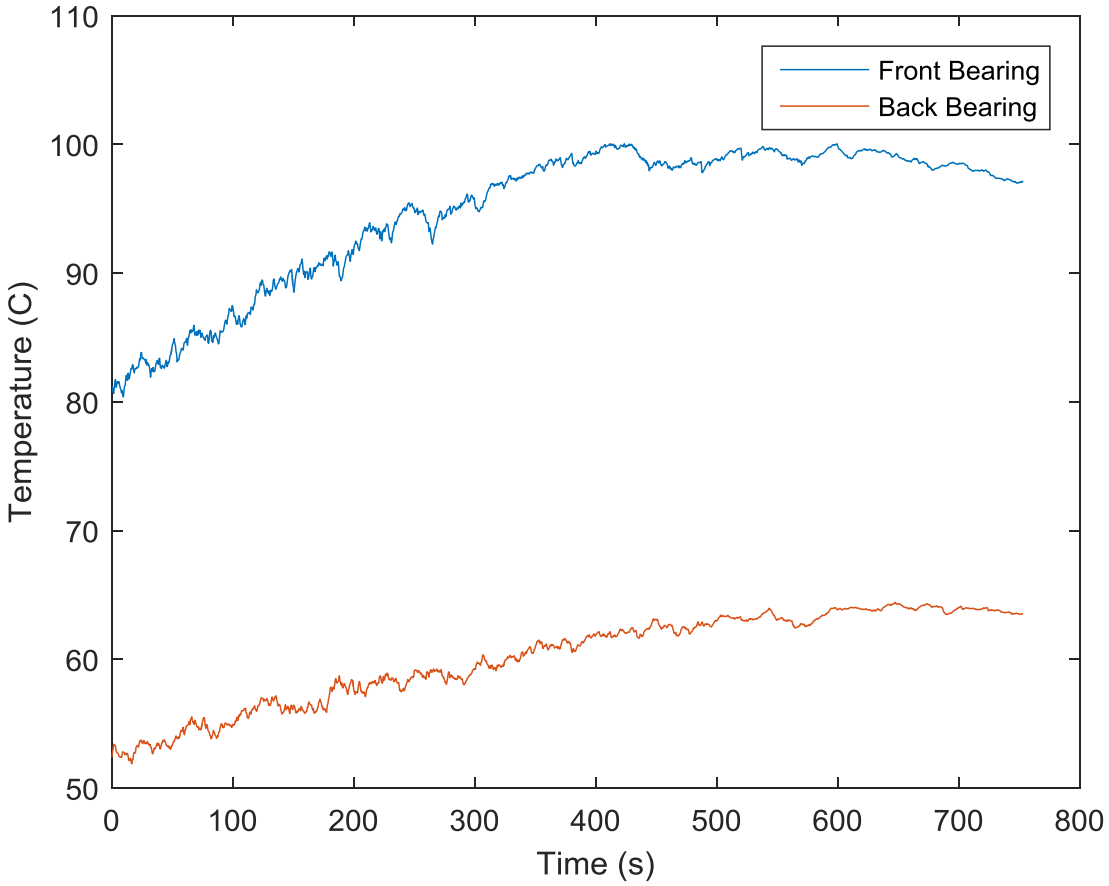

Figure 2.11: An example of temperature time histories measured at the front and back bearing cartridges of the sun gear shaft.

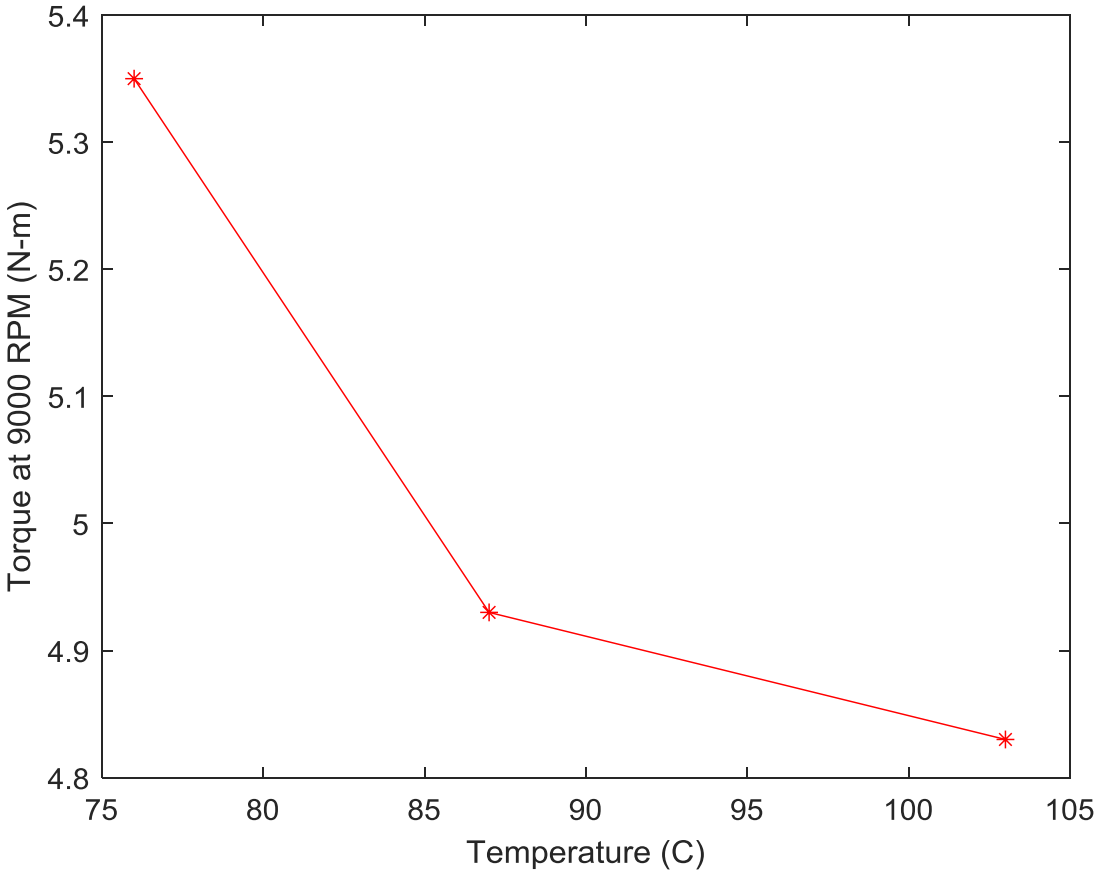

Figure 2.12: Variation of measured torque with the temperature of the front bearing cartridge of the sun gear at a speed of 9000 rpm

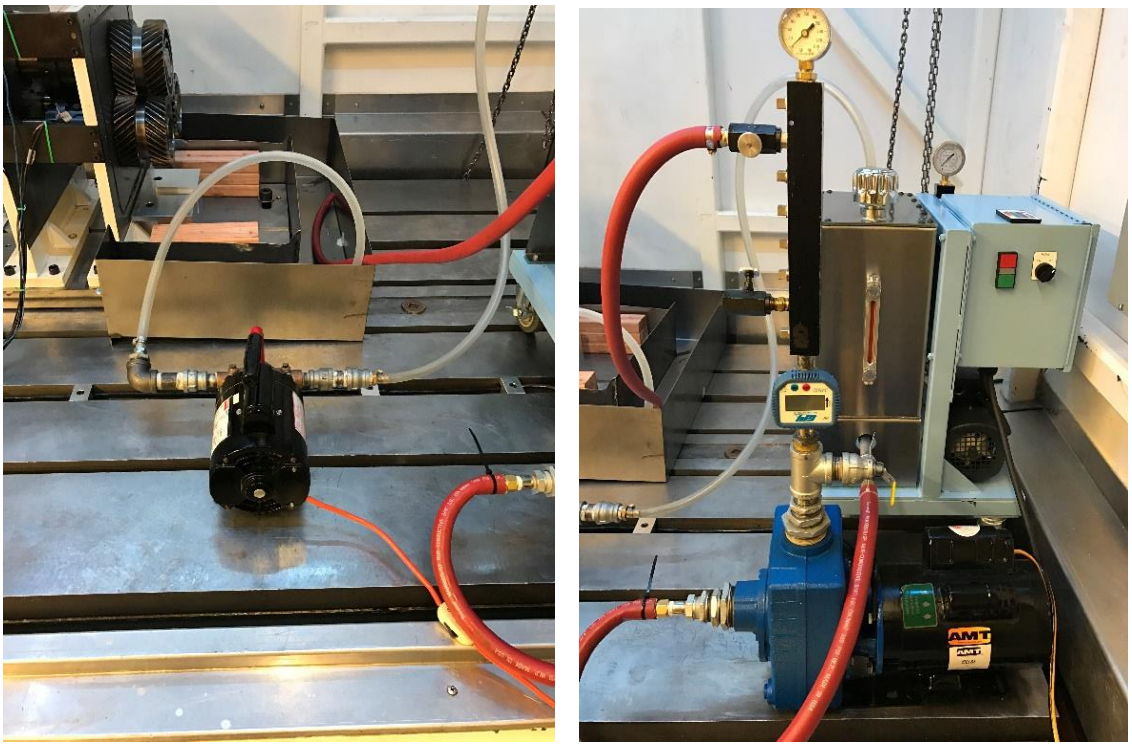

Figure 2.13: The lubrication system used in this study.

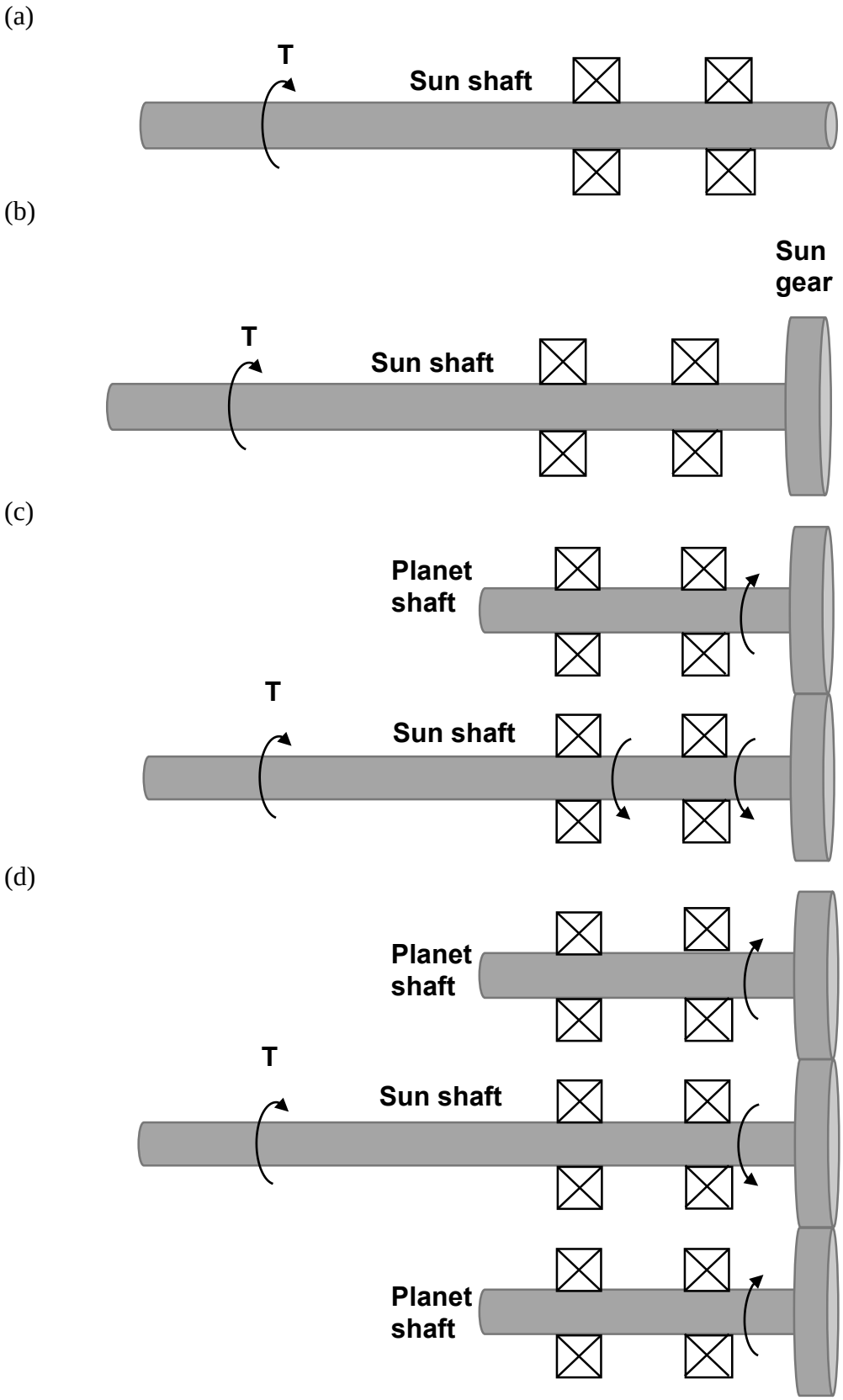

Figure 2.14: Four different test configurations used in this study.

Chapter 3

Experimental Results

3.1 Introduction

The main objective of this study was to develop an experimental methodology to measure load-independent losses of a turbofan gearbox. As reviewed in Chapter 2, this objective has been achieved. This methodology will be employed in further research to perform extensive experimental parametric studies. With this stated, this chapter presents some limited preliminary measurements collected using the same methodology for its demonstration. Furthermore, the power loss measurements P_I to P_{IV} as defined by Equations (2.5), (2.6), (2.10) and (2.15) will be used in manner described in Section 2.5 to attempt to determine the drag (sun and planet gears), bearing (sun and planet shafts) and gear mesh pocketing losses as afforded by the configurations defined in Table 2.1.

3.2 Power Loss Measurements

The measured normalized power losses $\bar{P}_I$, $\bar{P}_{II}$, $\bar{P}_{III}$ and $\bar{P}_{IV}$ obtained through testing of configurations I-IV of Figure 2.14 are compared in Figure 3.1 as a function of

inputs (sun) shaft speed Ω. As expected, configuration IV results in the largest power loss with the loss reducing with reduced content. For instance, at $\Omega = 4000$ rpm, $\bar{P}_{II} = 1.08\bar{P}_I$ indicating that the sun gear drag increased the power loss about 8% while this increase is 25% at $\Omega = 8000$ rpm. Comparison of measurements for configurations II and III indicates that adding a planet (its bearings, drag and the pocketing of the sun-planet mesh) results in $\bar{P}_{III} = 2.06\bar{P}_{II}$ (106% increase) at $\Omega = 4000$ rpm, and $\bar{P}_{III} = 2.11\bar{P}_{II}$ (a 111% increase) at $\Omega = 8000$ rpm. Similarly, configuration IV is observed to yield 28% and 37% increase from configuration III at $\Omega = 4000$ and 8000 rpm, respectively. This increase must represent the losses of the second planet (drag and its bearings) and the pocketing loss of the second gear mesh.

In regards to the sensitivity of the measured $\bar{P}_i$ ($i = I, II, III, IV$) to rotational speed Ω, exponential trend lines are evident in the form of $\bar{P}_i(\Omega) = a_i \Omega^{b_i}$. While the a_i values are of limited interest here since the power loss values have been normalized, the power of speed are seen to be $b_{IV} = 1.9$ for configuration IV while $b_I = 2.1$ for configuration I, suggesting that all power loss components have nearly a power of two relationship with Ω.

3.3 Power Loss Components

As outlined in Section 2.5, various tests can be compared under certain assumptions (such as sun and planet drag losses are equal, and sun and planet bearing losses are equal), it might be possible, at least in theory, to estimate the components of the power losses. For instance, comparing $\bar{P}_I$ and $\bar{P}_{II}$ values in Figure 3.1 according to Equations (2.5) and (2.6),

sun shaft bearing loss $P_b = P_{b,sf} + P_{b,sr} = P_I$ and sun drag loss $P_{s,d} = P_d = P_{II} - P_I$ can be estimated and compared to P_{II} in terms of the ratios $\bar{P}_b/\bar{P}_{II}$ and $\bar{P}_d/\bar{P}_{II}$. Figure 3.2 plots these ratios as a function of Ω. It is evident here that $\bar{P}_b/\bar{P}_{II}$ ranges from 0.95 to 0.75 suggesting that 95% to 75% of P_{II} is due to bearing losses with the remaining 5% to 25% due to the sun gear windage drag. It is seen that the percentage of sun drag loss increases with Ω.

A similar graph is presented in Figure 3.3 for configuration that shows the contributions of various components to $\bar{P}_{III}$. According to Equation (2.10), $\bar{P}_b/\bar{P}_{III}$ now includes both sun shaft bearing loss and those of the planet shaft. The drag component includes drag of both sun gear and one planet, and the pocketing loss component $\bar{P}_{sp,poc}/\bar{P}_{III}$ has pocketing loss of one gear mesh. At $\Omega = 9000$ rpm, for instance, $\bar{P}_b/\bar{P}_{III} = 0.70$, $\bar{P}_d/\bar{P}_{III} = 0.22$ and $\bar{P}_{sp,poc}/\bar{P}_{III} = 0.08$ suggesting that bearing loss is still the biggest contributor.

Using the same logic, Figure 3.4 shows the contributions of the components of $\bar{P}_{IV}$ from tests with configuration IV. At $\Omega = 9000$ rpm, for instance, $\bar{P}_b/\bar{P}_{IV} = 0.68$, $\bar{P}_d/\bar{P}_{IV} = 0.22$ and $\bar{P}_{sp,poc}/\bar{P}_{IV} = 0.10$, that are quite similar to that of Figure 3.3 for configuration III.

As a final check, power loss components estimated by using the approximate formulae given in Section 2.5 are used to reconstruct the $\bar{P}_{IV}$ according to Equation (2.15) and compared to the actual measured values in Figure 3.5. In spite of above

oversimplifying assumptions, the differences between actual and reconstructed $\bar{P}_{IV}$ values are well within 20% suggesting that there is merit to looking at power loss components to obtain the total loss.

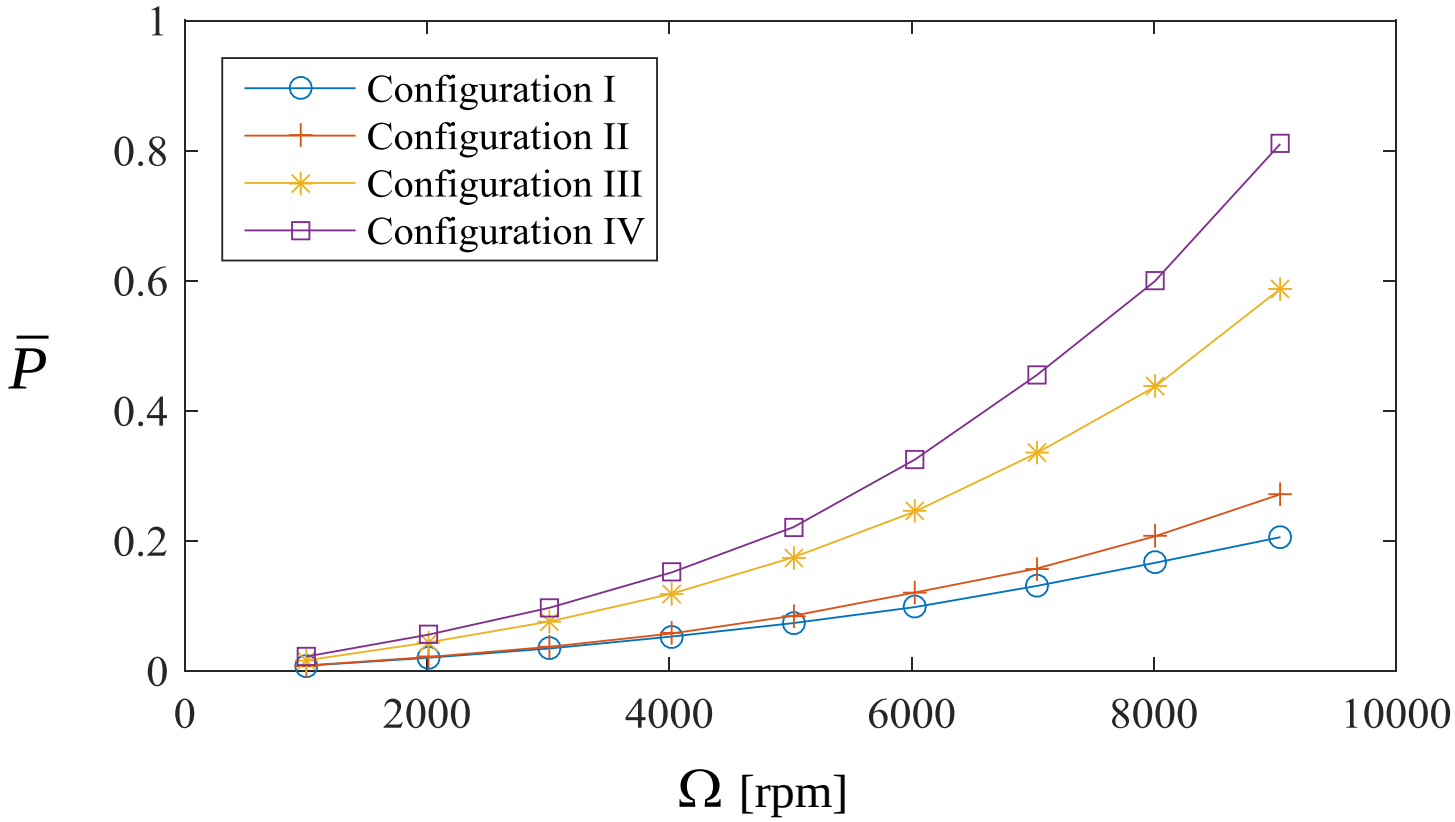

Figure 3.1: Measured normalized power loss values using configurations I to IV as a function of Ω.

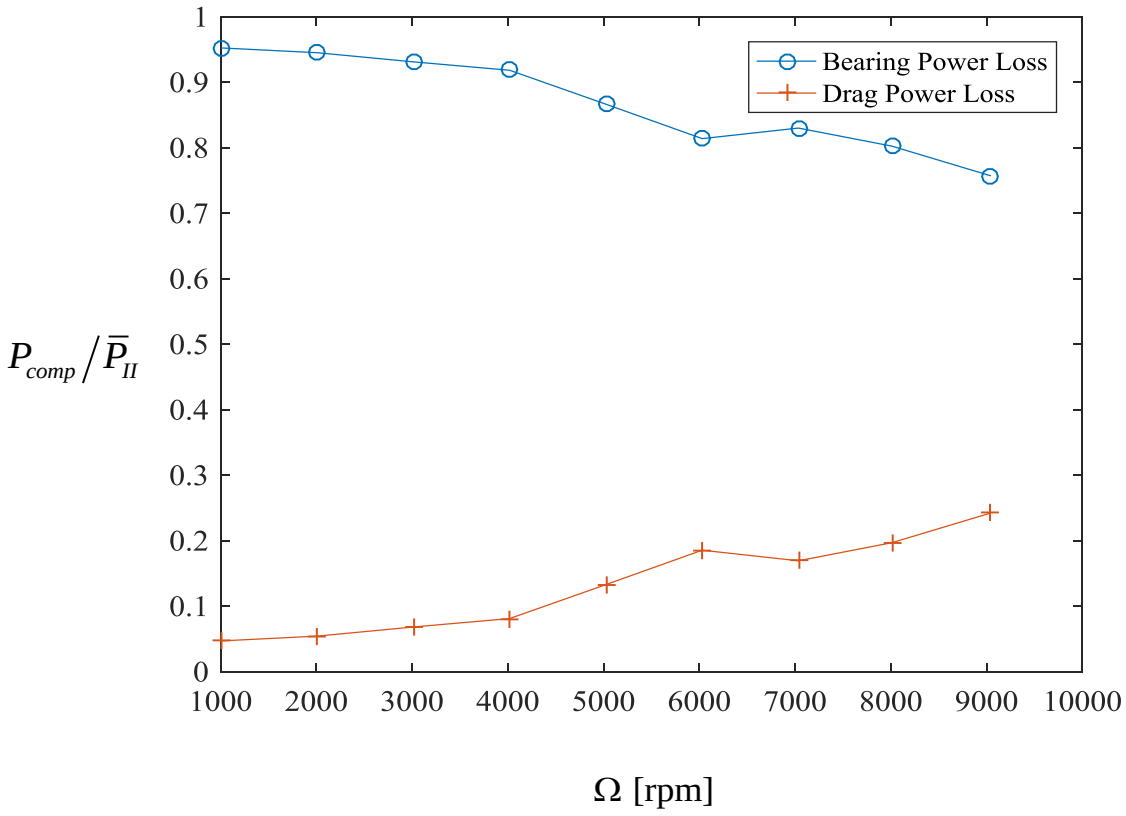

Figure 3.2: The bearing loss and sun gear drag loss components of measured $\bar{P}_{II}$ The vertical axis represents the component loss to total loss ratio $P_{comp}/\bar{P}_{II}$.

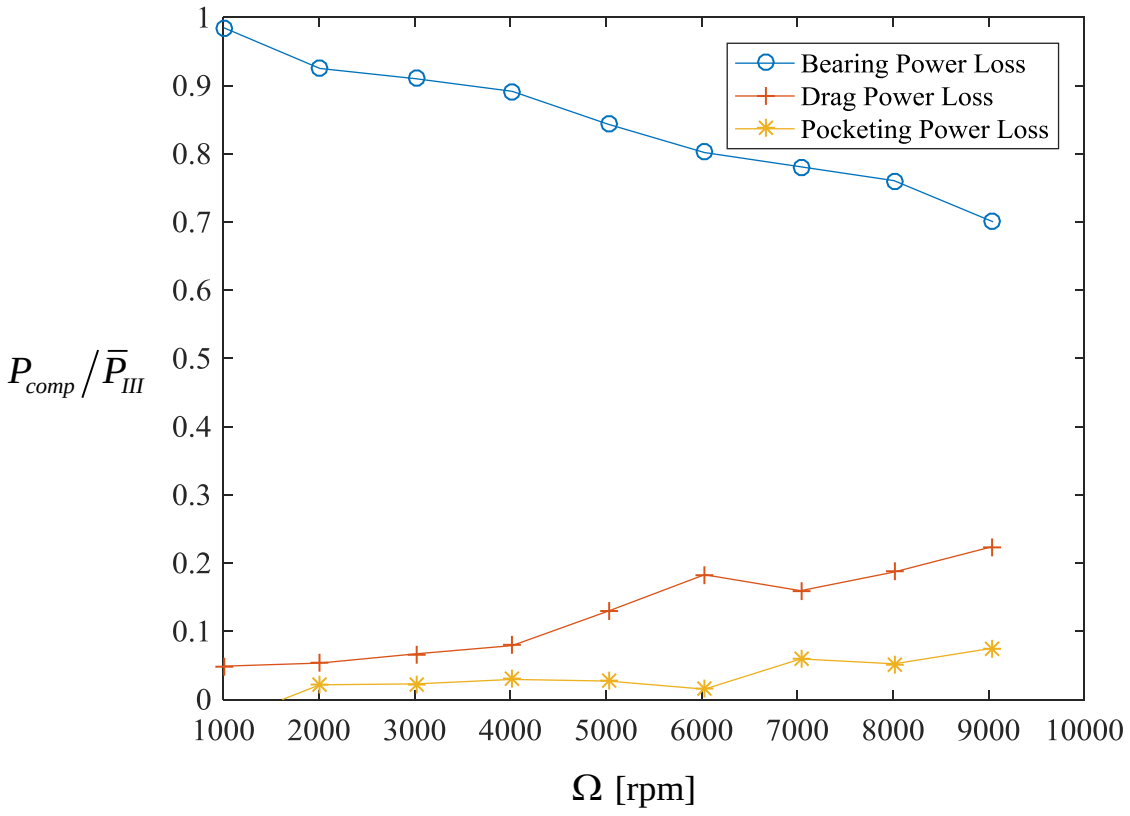

Figure 3.3: The bearing loss (sun and planet shaft) and gear drag loss (sun and planet gear) and pocketing loss components of measured $\bar{P}_{III}$ The vertical axis represent the component loss-to-total loss ratio $P_{comp}/\bar{P}_{III}$.

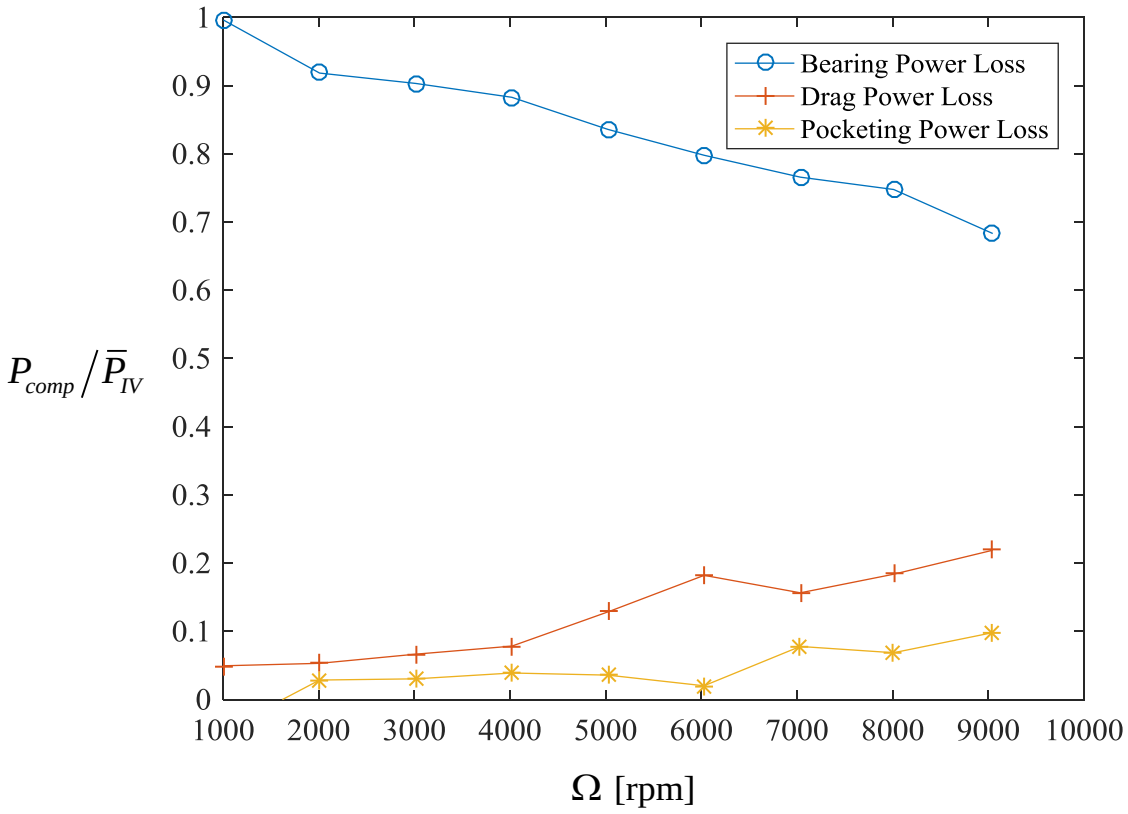

Figure 3.4: The bearing loss (sun shaft and two planet shafts) and gear drag loss (sun and two planet gears) and pocketing loss (two gear meshes) components of measured $\bar{P}_{IV}$ The vertical axis represents the component loss-to-total loss ratio $P_{comp}/\bar{P}_{IV}$

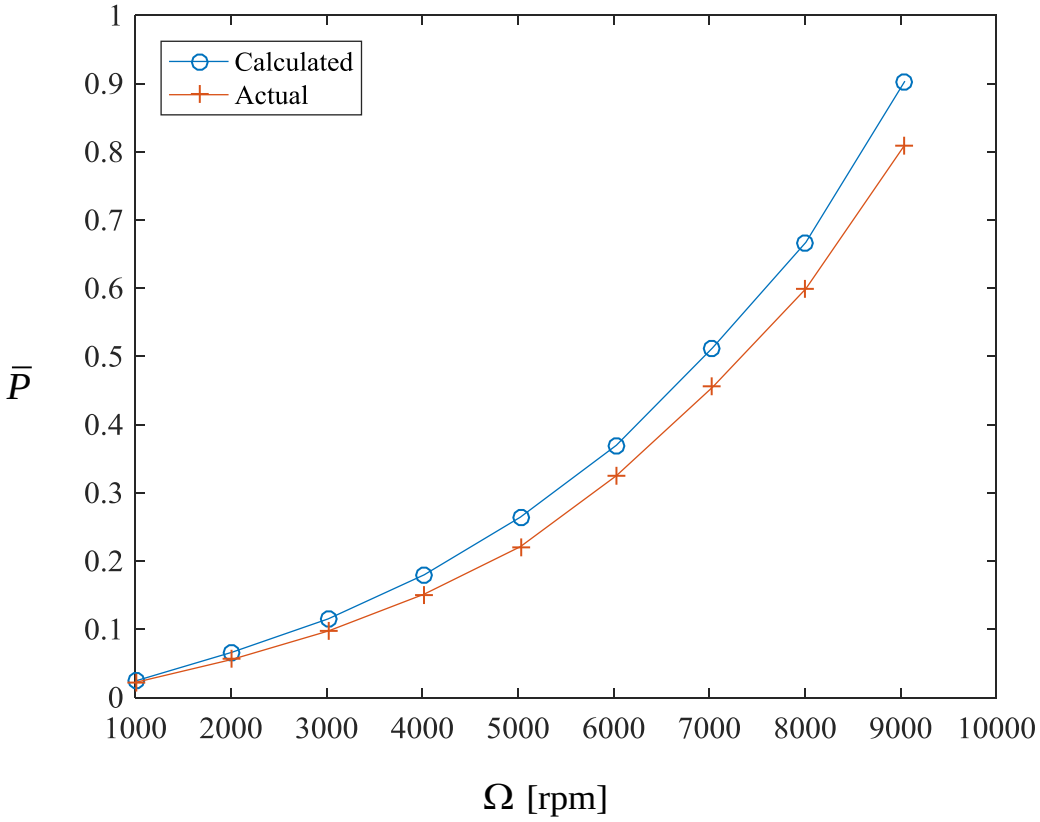

Figure 3.5: Comparison of measured $\bar{P}_{IV}$ values to those estimated as sum of the loss components.

Chapter 4

Conclusion

4.1 Summary

This preliminary investigation was performed in an attempt to quantify the spin power loss components of a high speed turbofan gearbox. The main focus of this study was to run various configurations of the testing set up to isolate the individual components of spin power loss. Once these components were determined, the measured power loss of the two planet configuration was compared to the calculated power loss using the individual spin loss components. The methodology developed in this investigation will be used in future studies on pocketing losses of a turbofan gearbox.

4.2 Major Conclusions

Based on the results discussed in chapter 3, the following conclusions of spin power losses for a turbofan gearbox can be made:

(i) Drag and pocketing power losses are significant only at higher speeds.

(ii) Bearing loss is the primary sources of spin power loss followed by drag and pocketing losses.

(iii) Pocketing loss is a large contributor of the spin power loss at higher speeds.

(iv) Summing power loss component measurements of a planetary gear set with two planet gears shows about 20% difference between the actual power loss and the sum of its components.

(v) Accuracy of the estimation for power loss components can be improved further by factoring in the size differences between the planet sub-assemblies and the sun sub-assemblies.

4.3 Future Work

This preliminary investigation forms the basis for an MS thesis on pocketing losses. The methodology and test setup used for this study will be further developed using real engine fluids at elevated temperatures and flow rates to perform:

(i) Measurements of pocketing pressures to validate pocketing loss models.

(ii) Experimental parametric studies on effect of root clearance on pocketing loss.

References

[1] D. Talbot and A. Kahraman, "A Methodology to Predict Power Losses of Planetary Gear Sets," *Int. Gear Conf. 2014 26th–28th August 2014, Lyon*, pp. 625–635, 2014.

[2] D. C. Talbot, A. Kahraman, and A. Singh, "An Experimental Investigation of the Efficiency of Planetary Gear Sets," *J. Mech. Des.*, vol. 134, no. 2, p. 21003, 2012.

[3] D. C. Talbot, A. Kahraman, and A. Singh, "An Experimental and Theoretical Investigation of the Efficiency of Planetary Gear Sets," The Ohio State University, 2012.

[4] A. Kahraman, D. R. Hilty, and A. Singh, "An Experimental Investigation of Spin Power Losses of a Planetary Gear Set," *Mech. Mach. Theory*, vol. 86, pp. 48–61, 2015.

[5] D. C. Talbot, A. Kahraman, and S. Seetharaman, "A Pocketing Power Loss Model for Helical Gears," *J. Tribol.*, vol. 136, no. 21105, 2014.

[6] T. Harris, *Rolling Bearing Analysis*, 3rd ed. New York: John Wiley & Sons inc., 1991.

[7] P. M. Wild, N. Djilali, and G. W. Vickers, "Experimental and Computational Assessment of Windage Losses in Rotating Machinery," *Trans. ASME*, vol. 118, no. March, pp. 116–122, 1996.

[8] L. S. Akin, D. P. Townsend, and J. J. Mross, “Technical Memorandum Study of Lubricant Jet Flow Phenomena in Spur Gears,” 1974.

[9] P. H. Dawson, “Windage Loss in Larger High-Speed Gears,” *Arch. Proc. Inst. Mech. Eng. Part A Power Process Eng. 1983-1988 (vols 197-202)*, vol. 198, no. 1, pp. 51–59, 2006.

[10] Y. Diab, F. Ville, and P. Velex, “Investigations on Power Losses in High-Speed Gears,” *Proc. Inst. Mech. Eng. Part J J. Eng. Tribol.*, vol. 220, no. 3, pp. 191–198, 2006.

[11] S. Seetharaman and A. Kahraman, “Load-Independent Spin Power Losses of a Spur Gear Pair: Model Formulation,” *J. Tribol.*, vol. 131, no. 2, p. 22201, 2009.

[12] Y. Diab, F. Ville, H. Houjoh, P. Sainsot, and P. Velex, “Experimental and Numerical Investigations on the Air-Pumping Phenomenon in High-Speed Spur and Helical Gears,” *Proc. Inst. Mech. Eng. Part C J. Mech. Eng. Sci.*, vol. 219, no. 8, pp. 785–800, 2005.

[13] D. R. Hilty, “An Experimental Investigation of Spin Power Losses of a Planetary Gear Set,” *Components*, pp. 1–94, 2010.

[14] “Gearing Up for Geared Turbofans,” 2009. [Online]. Available: http://machinedesign.com/mechanical-drives/gearing-geared-turbofans. [Accessed: 03-Jan-2017].